

The $\vec{d}p \rightarrow {}^3\text{He} \pi^0$ reaction near threshold

V. N. Nikulin,^{1,2,3} A. Boudard,¹ M. Clajus,⁴ B. Fabbro,¹ M. Garçon,¹
 R. S. Kessler,⁴ L. K. Lytkin,^{2,5} B. Mayer,^{1*} B. M. K. Nefkens,⁴ F. Plouin,² J. Poitou,¹ E. Tomasi-Gustafsson,²
 W. T. H. van Oers,⁶ D. White,⁴ and C. Wilkin⁷

¹*Service de Physique Nucléaire, CEA Saclay, F-91191 Gif-sur-Yvette, France*

²*Laboratoire National Saturne, F-91191 Gif-sur-Yvette, France*

³*St. Petersburg Nuclear Physics Institute, 188350 Gatchina, Russia*

⁴*Department of Physics, University of California, Los Angeles, California 90095*

⁵*Joint Institute for Nuclear Research, Dubna, Russia*

⁶*TRIUMF, 4004 Wesbrook Mall, Vancouver, British Columbia, Canada V6T 2A3*

⁷*University College London, London WC1E 6BT, United Kingdom*

(Received 17 May 1996)

Angular distributions for the differential cross section and three deuteron analyzing powers iT_{11} , T_{20} , and T_{22} of the reaction $\vec{d}p \rightarrow {}^3\text{He} \pi^0$ have been measured over the whole angular domain at 20 energies close to threshold ($0.03 < T_{\pi}^{\text{c.m.}} < 10.2$ MeV). The differential cross section and tensor analyzing power T_{20} both show strong variation in energy and angle due to interference between S - and P -wave pion production, whereas iT_{11} and T_{22} remain consistent with zero over the whole experimental range. All the data at different energies and angles fall on universal curves when plotted as functions of the single variable $p_{\pi} \cos \Theta$, evaluated in the c.m. The broad features of the results are in line with theoretical expectations. [S0556-2813(96)02710-0]

PACS number(s): 25.40.Qa, 25.45.-z, 24.70.+s, 25.10.+s

I. INTRODUCTION

Studies of pion production by protons on nuclei have shown the reactions to be generally dominated by the formation of the P -wave $\Delta(1232)$ isobar. To identify the small but interesting S -wave production, experiments must be carried out very close to threshold. However, even in the case of an inverse reaction involving the capture from the orbits of pionic atoms, which corresponds to very low energies, the Δ quickly becomes dominant as the nuclear size increases. The strength of the P -wave interaction is such that the details of the reaction mechanism are then lost through multiple scattering. The only hope of isolating S -wave production, and seeing the direct effects of the reaction mechanisms, is by studying near-threshold production on very light nuclei.

The prototype pion production reaction is $pp \rightarrow d\pi^+$ and there have been countless experimental and theoretical studies of this and the inverse process reported in the literature. The low-energy total cross section is usually parametrized in the form

$$\sigma(pp \rightarrow d\pi^+) = 2\sigma(np \rightarrow d\pi^0) = \alpha\eta + \beta\eta^3, \quad (1)$$

where $\eta = p_{\pi}/m_{\pi}$ is the pion c.m. momentum in pion mass units. The parameters α and β primarily reflect S - and P -wave pion production and have been determined to be $\alpha = 184 \pm 5 \mu\text{b}$ and $\beta = 781 \pm 79 \mu\text{b}$ [1]. The P -wave contribution becomes as large as that of the S at a pion c.m. kinetic energy of about 15 MeV.

There is no interference between pion S and P waves in the total cross section and, because the initial protons are identical, such interference terms are also absent from the

unpolarized differential distribution. As a consequence the differential cross section is of the form $1 + \gamma\eta^2 \cos^2 \Theta$, with γ evolving only gradually with energy.

The lightest nucleus for which S - and P -wave pion production can have an interference effect in the differential cross section, and hence give useful phase information, involves the $p d \rightarrow {}^3\text{He} \pi^0$ reaction and in this case the effects are enormous. It has been shown at IUCF [2] that for a pion c.m. kinetic energy of only 2.7 MeV, forward and backward pion productions differ by about a factor of 5.

The existence of a strong forward-backward asymmetry near threshold was confirmed in measurements at LNS [3,4]. These $\vec{d}p \rightarrow {}^3\text{He} \pi^0$ experiments were carried out in the forward and backward directions in the center-of-mass system using a tensor-polarized deuteron beam. Spin-one observables are much richer than spin-half observables and the experiments showed that not only the cross section but also the deuteron tensor analyzing power T_{20} varied violently near threshold. This is the only analyzing power which does not vanish in the forward-backward directions and it there measures the difference between the cross sections for deuterons with helicities $m = \pm 1$ and $m = 0$,

$$T_{20} = \frac{1}{\sqrt{2}} \left(\frac{\sigma(m=1) + \sigma(m=-1) - 2\sigma(m=0)}{\sigma(m=1) + \sigma(m=-1) + \sigma(m=0)} \right). \quad (2)$$

The reaction was investigated phenomenologically by Germond and Wilkin [5], who showed that for collinear kinematics there are only two independent scattering amplitudes, A corresponding to $m=0$ and B to $m=\pm 1$. It is then possible to extract the magnitudes of these amplitudes from the LNS data [3,4] on analyzing power and c.m. differential cross sections through

*Electronic mail: mayer@phnx7.saclay.cea.fr

$$\begin{aligned}
 |A|^2 &= \frac{p_p}{p_\pi} (1 - \sqrt{2}T_{20}) \frac{d\sigma}{d\Omega}, \\
 |B|^2 &= \frac{p_p}{p_\pi} (1 + T_{20}/\sqrt{2}) \frac{d\sigma}{d\Omega},
 \end{aligned} \quad (3)$$

where p_p and p_π are the c.m. momenta of the proton and pion, respectively.

One feature of the Germond-Wilkin model is the prediction that at low energies in the forward and backward directions both $|B|^2$ and $|A|^2$ should be essentially quadratic functions of $\eta = p_\pi/m_\pi$. This feature is well reproduced by the data [2,3] and the dramatic variation of T_{20} with energy is in part a reflection of the much smoother polynomial dependence present in the amplitudes A and B .

In order to study the process in more depth, the $\vec{d}p \rightarrow {}^3\text{He} \pi^0$ reaction was measured in 20 energy steps close to threshold and over the whole angular domain. In addition to the cross section and T_{20} , the deuteron vector analyzing power iT_{11} and a second tensor analyzing power T_{22} , both of which vanish in the forward direction, were also determined. This is the largest data set ever measured in a single pion production experiment and it is hoped that this will help to elucidate the dynamics and constrain further any theoretical model. Even though this is clearly insufficient for a full amplitude analysis, the present results become strikingly simple when all data at different energies and angles are plotted as a function of the global variable $\eta \cos\Theta$ and the consequences of this are explored in the results and conclusions.

II. EXPERIMENTAL METHOD

The experiment was carried out at the Laboratoire National SATURNE (LNS), Saclay, France, using a polarized deuteron beam [6] incident on a 7 mm thick liquid hydrogen target. The beam intensity, which was monitored by two scintillation counter telescopes viewing a 40 μm thick Kapton foil placed 1 m upstream of the target, was calibrated using the carbon activation method [7]. The beam polarization, which was axially symmetric, is characterized by two numbers ρ_{10} and ρ_{20} , which are, respectively, the vector and tensor polarizations. These were measured between data-taking runs with a low-energy polarimeter prior to acceleration of the deuterons in the SATURNE synchrotron. Subsequent depolarization during the beam acceleration and extraction has been proved to be negligible [6].

The recoil particles were detected in the SPES2 magnetic spectrometer [8], positioned at zero degrees with respect to the incident beam direction. The spectrometer consists of a quadrupole, two dipoles, and a detection system formed of three multiwire proportional chambers (MWPC's), with two wire planes each ($U \times V$), 2 mm wire spacing, equipped with PCOS3 readout systems, and of two layers of plastic scintillation counters A and B placed 1.6 m apart. A coincidence between the two scintillator planes produced a trigger for the acquisition system and the time of flight from A to B and the energy deposited in hodoscope A were also recorded to ensure a proper identification of the ${}^3\text{He}$ nuclei. Further details on the experimental setup can be found in Ref. [8].

The threshold of the reaction is at a beam energy of 397.24 MeV. The measurements were carried out at 20 beam energy settings, from 397.35 MeV up to 429.75 MeV, covering the range in η from 0.02 to 0.389. A measurement below threshold, at 396 MeV, was performed in order to monitor the shapes of background spectra. To permit a proper subtraction of the contribution from the target cell windows, measurements were carried out with an identical target cell containing only gaseous hydrogen. These measurements will be referred to as empty-target runs.

Since the incident deuteron energy is very close to the production threshold, the reaction products have small momenta in the c.m. frame. As a consequence the recoil ${}^3\text{He}$ particles are emitted within a narrow cone around the beam axis and in a relatively small momentum band, centered at 1250 MeV/c. The maximum beam energy was chosen so as to ensure the detection of all the ${}^3\text{He}$ within the momentum and angular acceptances of SPES2. Having determined the momentum and angle of the recoil ${}^3\text{He}$ in the SPES2 spectrometer, the $\vec{d}p \rightarrow {}^3\text{He} \pi^0$ reaction was identified.

The analyzing powers were determined from the dependence of the counting rates on the beam polarization parameters ρ_{10} and ρ_{20} ,

$$\begin{aligned}
 N(\Theta, \varphi) &\propto \{1 \pm \sqrt{2}\rho_{10}iT_{11}(\Theta)\cos\varphi \\
 &\pm \rho_{20}[T_{20}(\Theta)/2 + \sqrt{3/2}T_{22}(\Theta)\cos 2\varphi]\}, \quad (4)
 \end{aligned}$$

where Θ denotes the angle between the ${}^3\text{He}$ and the deuteron in the c.m. frame and φ the azimuthal angle. The SATURNE synchrotron provides beam bursts sequentially in four different states of the beam polarization and the \pm signs refer to independent reversals of the vector and tensor polarizations.

III. DATA ANALYSIS

The principal stages in the data analysis were the ${}^3\text{He}$ identification and trajectory reconstruction, the use of the ${}^3\text{He}$ momentum distribution in order to determine the precise beam energy and the total cross section, and the determination of the c.m. angles Θ and φ for each event, necessary for the extraction of angular distributions of the cross sections and analyzing powers.

A. ${}^3\text{He}$ identification and trajectory reconstruction

Loose cuts in the amplitude and time spectra for the scintillators A and B were applied in order to select ${}^3\text{He}$ events. After the momentum analysis in the magnetic spectrometer, the identification is unambiguous, as can be seen from Fig. 2 of Ref. [8].

The trajectory reconstruction algorithm required that at least two out of the three MWPC planes be hit (for each direction U and V), with at most one plane having multiple hits when three planes were involved. In the latter case, the trajectory yielding the best alignment between the three planes was selected. The fraction of nonreconstructible events was monitored separately for each counter of the A hodoscope, in order to keep track of possible position-dependent inefficiencies. This fraction was at the level of 3–5%. For reconstructible events, a track alignment condi-

tion was applied; events where the measured position in the middle MWPC differed by more than 1.25 mm from the position inferred from the other two MWPC's were discarded. The efficiency of this tight cut, of the order of 85%, was well controlled and very stable for all runs and beam polarization states.

The momentum and angles of ^3He nuclei at the entrance of the spectrometer were calculated using first-order optics. It was checked by ray tracing through measured magnetic fields that this was a very good approximation. In the following, the variable δ will denote the relative change of momentum with respect to its central value at a given energy.

B. Analysis of the ^3He momentum distributions

Near threshold, the width of the ^3He momentum spectrum ($\equiv 2\delta_{\text{max}}$) is proportional to $\eta = p_\pi/m_\pi$. This allows us to determine the deuteron beam energy with a far better accuracy than that given by the accelerator parameters. Furthermore, to a very good accuracy, the c.m. angle is given by the relation

$$\cos\Theta = \delta/\delta_{\text{max}}. \quad (5)$$

The shape of the observed momentum distributions, the above relation between momentum and c.m. angle, and the expected behavior of the differential cross section as a quadratic function of $\cos\Theta$ suggested a parametrization of the δ distribution in the form

$$N(\delta) \propto \int_{-\delta_{\text{max}}}^{\delta_{\text{max}}} R(\delta' - \delta)(1 + a\delta' + b\delta'^2)d\delta'. \quad (6)$$

The shape of the resolution function R was inferred from Monte Carlo simulations. The main contribution to the momentum resolution comes from the energy loss of the ^3He 's in the target cell, which depends on the position of the reaction vertex along the beam direction. As a consequence R is dominantly a rectangular distribution, smeared asymmetrically due to the tail of the energy-loss distribution on the low-energy side. The integral in Eq. (6) was approximated numerically. The momentum distributions were then very well described by a nine-parameter fit involving δ_{max} , an offset parameter δ_0 , cross section parameters a and b , the total number of events, and two parameters for the shape of R and two for the linear background. An example of this is illustrated in Fig. 1. In fits to the experimental data, the parameters a and b turned out to be nearly energy independent and the physical meaning of this finding will be discussed in Sec. V.

In the run closest to threshold, the beam energy loss in the liquid hydrogen (about 70 keV/mm plus fluctuations) meant that the $d p \rightarrow ^3\text{He} \pi^0$ reaction could not occur near the end of the target, thus decreasing the width of the resolution function R . This effect was taken into account by a proper parametrization of the observed spectra and an effective target length was used in the cross section calculations for these runs. For the three lowest-energy runs, the parameters a and b could not be determined and they were assumed to be constant, with their values taken from the higher-energy runs.

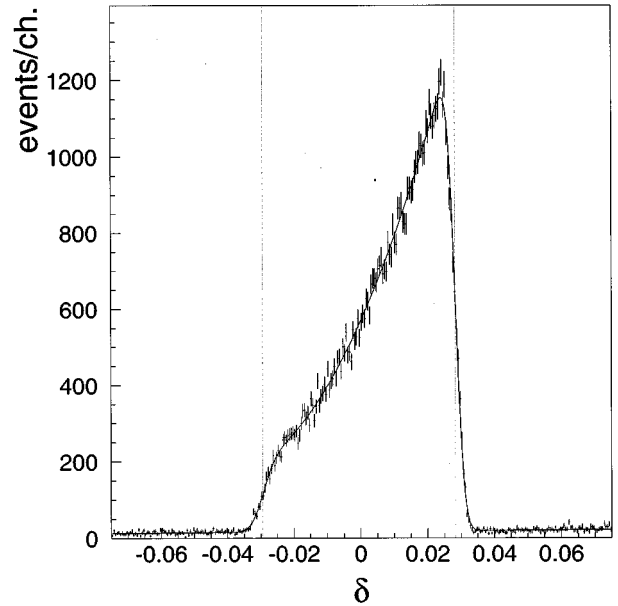


FIG. 1. Experimental δ spectrum at $T_{\text{beam}} = 410$ MeV, with a fitted curve. The vertical dotted lines correspond to the kinematical limits $\pm\delta_{\text{max}}$.

The total cross sections and the beam energies at the center of the target were deduced from the ^3He momentum distributions and their parametrization. An analysis of these spectra for different beam polarization states allowed the extraction of an average tensor analyzing power T_{20} , as shown in Sec. IV.

C. Determination of c.m. angles

For each event, the trajectory reconstruction gave a determination of the ^3He momentum and the projected reaction angles in the x and y directions in the laboratory frame, ϑ_x and ϑ_y . From the comparison of Monte Carlo simulations to the data, the resolutions (one standard deviation) in these three variables were estimated to be 0.2%, 2 mr, and 12 mr, respectively. For a two-body reaction, the momentum and angle $\vartheta \equiv \sqrt{\vartheta_x^2 + \vartheta_y^2}$ are correlated and provide redundant information to determine the c.m. angle Θ . Therefore, a kinematical fit was performed to extract Θ , using the above resolutions and the beam energy extracted as in Sec. III B. Since the value of ϑ_y is poorly defined, whereas the laboratory angle ϑ is well determined from δ , the azimuthal angle φ was evaluated from the ratio ϑ_x/ϑ . Ambiguity in the sign of ϑ_y is irrelevant for $\cos\varphi$ and $\cos 2\varphi$ distributions. For the determination of the analyzing powers $iT_{11}(\Theta)$, $T_{20}(\Theta)$, and $T_{22}(\Theta)$, the data were binned in azimuthal angle with $\Delta\varphi = 45^\circ$.

D. Background subtraction

For each angular bin and each polarization state, an empty target contribution, properly normalized using the monitor information, was subtracted. A further subtraction of the residual background was performed by rejecting events with $\chi_{kf}^2 > 10$ in the above-mentioned kinematical fit. Events with $\chi_{kf}^2 > 10$ were uniformly distributed in the δ spectra. The

TABLE I. Total cross sections and average T_{20} . The errors do not include an overall systematic normalization uncertainty of 8% in the cross sections and 3% in T_{20} .

T_d (MeV)	η	σ_T (μb)	T_{20}
397.35	0.022 ± 0.013	0.32 ± 0.03	-1.33 ± 0.06
397.75	0.048 ± 0.007	0.96 ± 0.05	-1.29 ± 0.06
398.75	0.082 ± 0.004	1.42 ± 0.05	-1.29 ± 0.03
399.75	0.106 ± 0.003	1.86 ± 0.04	-1.34 ± 0.06
400.75	0.126 ± 0.003	2.04 ± 0.04	-1.22 ± 0.06
402.15	0.149 ± 0.002	2.54 ± 0.04	-1.27 ± 0.05
405.75	0.197 ± 0.002	3.20 ± 0.04	-1.31 ± 0.04
407.75	0.219 ± 0.002	3.70 ± 0.07	-1.34 ± 0.06
409.75	0.239 ± 0.002	3.91 ± 0.08	-1.29 ± 0.07
410.75	0.248 ± 0.002	4.28 ± 0.09	-1.28 ± 0.07
411.75	0.258 ± 0.001	4.20 ± 0.07	-1.29 ± 0.06
412.75	0.266 ± 0.001	4.56 ± 0.09	-1.22 ± 0.07
413.75	0.275 ± 0.001	4.71 ± 0.08	-1.29 ± 0.06
414.75	0.283 ± 0.001	5.01 ± 0.09	-1.34 ± 0.06
415.75	0.292 ± 0.001	5.10 ± 0.09	-1.25 ± 0.06
417.75	0.307 ± 0.001	5.19 ± 0.10	-1.30 ± 0.07
419.75	0.322 ± 0.001	5.59 ± 0.13	-1.19 ± 0.08
421.75	0.336 ± 0.001	6.01 ± 0.15	-1.29 ± 0.09
424.75	0.357 ± 0.001	6.29 ± 0.12	-1.32 ± 0.07
429.75	0.389 ± 0.001	6.86 ± 0.17	-1.22 ± 0.09

χ_{kf}^2 distribution of the rejected events was extrapolated within the region of good events ($\chi_{kf}^2 < 10$) to estimate a residual background of the order of 1%. The loss of good events was calculated with a Monte Carlo simulation, which reproduced very well the shape of the distribution. This loss ranged between 0.3% and 1.5% and it was verified that this had essentially the same angular distribution as that of the final differential cross section.

IV. RESULTS

A. Total cross sections and T_{20}

In addition to the above-mentioned corrections (efficiencies of track reconstruction, of alignment and χ_{kf}^2 cuts, and use of effective target length for runs very close to threshold), the cross sections were corrected for nuclear interactions of the ${}^3\text{He}$'s in the target and in the components of SPES2. This correction amounted to 3%, independent of the ${}^3\text{He}$ momentum.

A relative monitoring error of 1% was added in quadrature with the statistical errors, to allow for possible systematic effects when comparing runs at different energies.

The numerical data for total cross sections and T_{20} are presented in Table I. Not included in the quoted errors is an overall systematic normalization error of 8% in the cross sections, coming mostly from uncertainties in the calibration method of the beam intensity and in the target thickness. There is also an overall 3% uncertainty in the T_{20} , due to systematic and statistical errors in the beam polarization measurements [6].

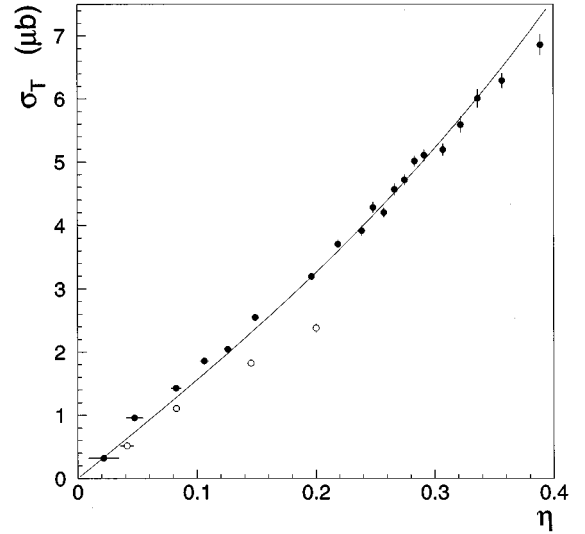


FIG. 2. Total cross section σ_T , for the $d p \rightarrow {}^3\text{He} \pi^0$ reaction, plotted as function of η . Solid circles are the results of the present experiment whereas the open circles are IUCF data [2]. The curve represents the global fit of Eq. (12).

As can be seen from Fig. 2, the cross section data from IUCF [2] are significantly lower than the present results by 20–25%, the discrepancy becoming larger with increasing η . This is much more than the claimed normalization uncertainties of 10% and 8%. The experimental techniques were very different and the origin of the discrepancy is not understood. The IUCF experiment used a thin CD_2 target, requiring a coincidence between the ${}^3\text{He}$ and two photons from π^0 decay.

The T_{20} values, which correspond to cross-section-weighted averages over angles, are relatively large, being consistent with a constant -1.290 ± 0.012 . This result is in good agreement with a previous measurement at $T_{\text{beam}} = 400.7$ MeV, which found -1.312 ± 0.039 [3].

B. Angular distributions of cross sections and analyzing powers

The differential cross sections are readily obtained from the analysis presented in Sec. III by summing the bins in the azimuthal angle. In addition to the systematic errors already discussed, errors in the parameters δ_0 and δ_{max} could affect the angular distributions by as much as 5% in the extreme bins near $\cos\Theta = \pm 1$, though the effect is negligible elsewhere.

The complete set of differential cross sections is presented in Fig. 3, where it is seen that the angular distributions are quite similar to those of the IUCF data [2] for the same η . In particular our data confirm the rapid rise of the forward-backward asymmetry as η increases.

The analyzing powers were extracted from the expected φ distribution of the counting rates using Eq. (4). Since the vector and tensor polarizations of the beam were reversed alternately in each of the four consecutive polarization states, three independent combinations of the counts in these four polarization states were considered for every (Θ, φ) bin (see Ref. [6] for details). One of these ratios is proportional to $\cos\varphi$, the proportionality coefficient yielding $iT_{11}(\Theta)$. A second one is fit to the expected linear dependence on

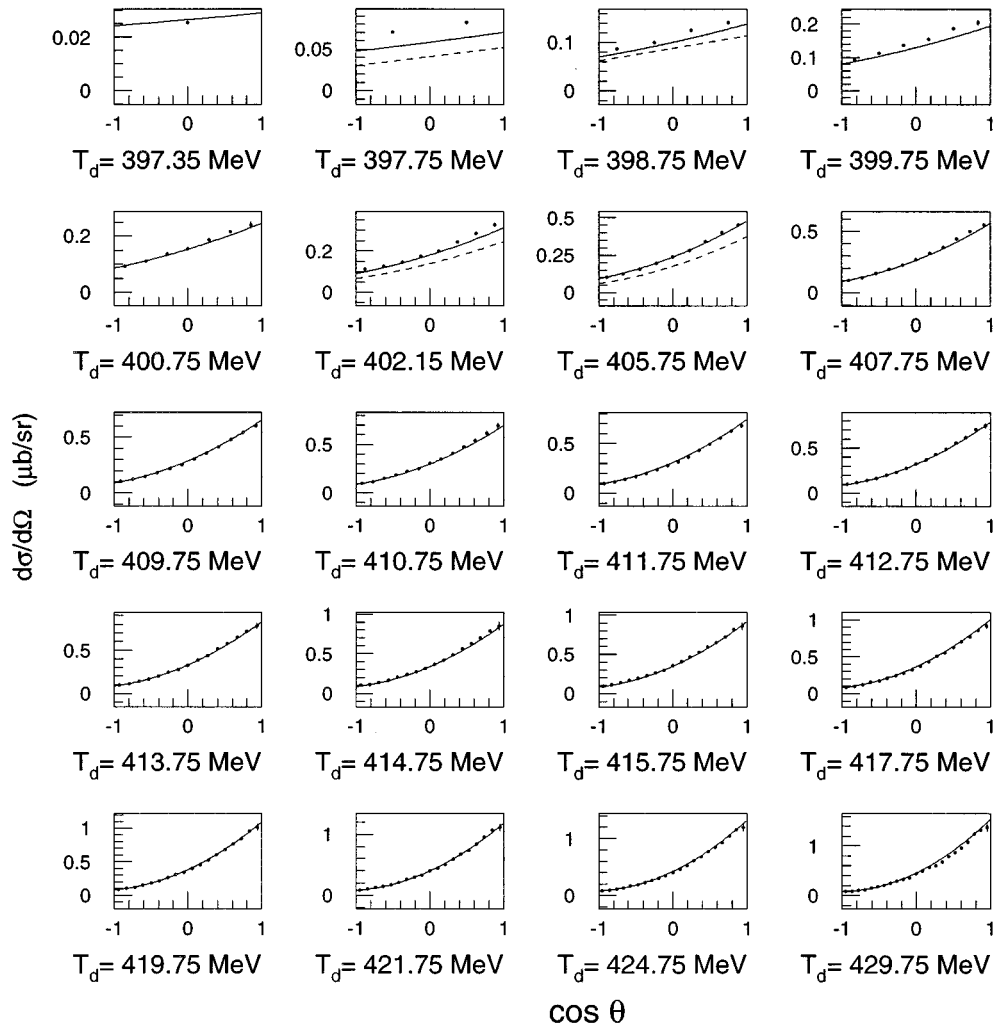


FIG. 3. Complete set of the differential cross section compared with curves representing the global fit of Eq. (8). The dashed curves are the fits of IUCF data [2] at neighboring values of η .

$\cos 2\varphi$ to give $T_{20}(\Theta)$ and $T_{22}(\Theta)$ separately. The third one should be identically zero and is used as a consistency check. The systematic error arising from uncertainty in the beam vector polarization is about 4%.

The angular distributions of the cross sections and the four analyzing powers measured are shown in Figs. 3–6.

V. PARAMETRIZATION AND INTERPRETATION OF THE DATA

The present data show clearly that the differential cross section and tensor analyzing power T_{20} for the $\vec{d}p \rightarrow {}^3\text{He}\pi^0$ reaction vary very strongly in energy and angle near threshold but that, in contrast, the two other analyzing powers that were measured, iT_{11} and T_{22} , are both compatible with zero everywhere. It should, however, be noted that the IUCF group [2] claims a small but nonzero proton analyzing power A_y . Since six complex amplitudes are required to describe the reaction, the present data set is incomplete and one must rely on guidance from theoretical models to interpret the results.

The spectator nucleon model of Germond and Wilkin [5] gives estimates for the values of the amplitudes A and B of

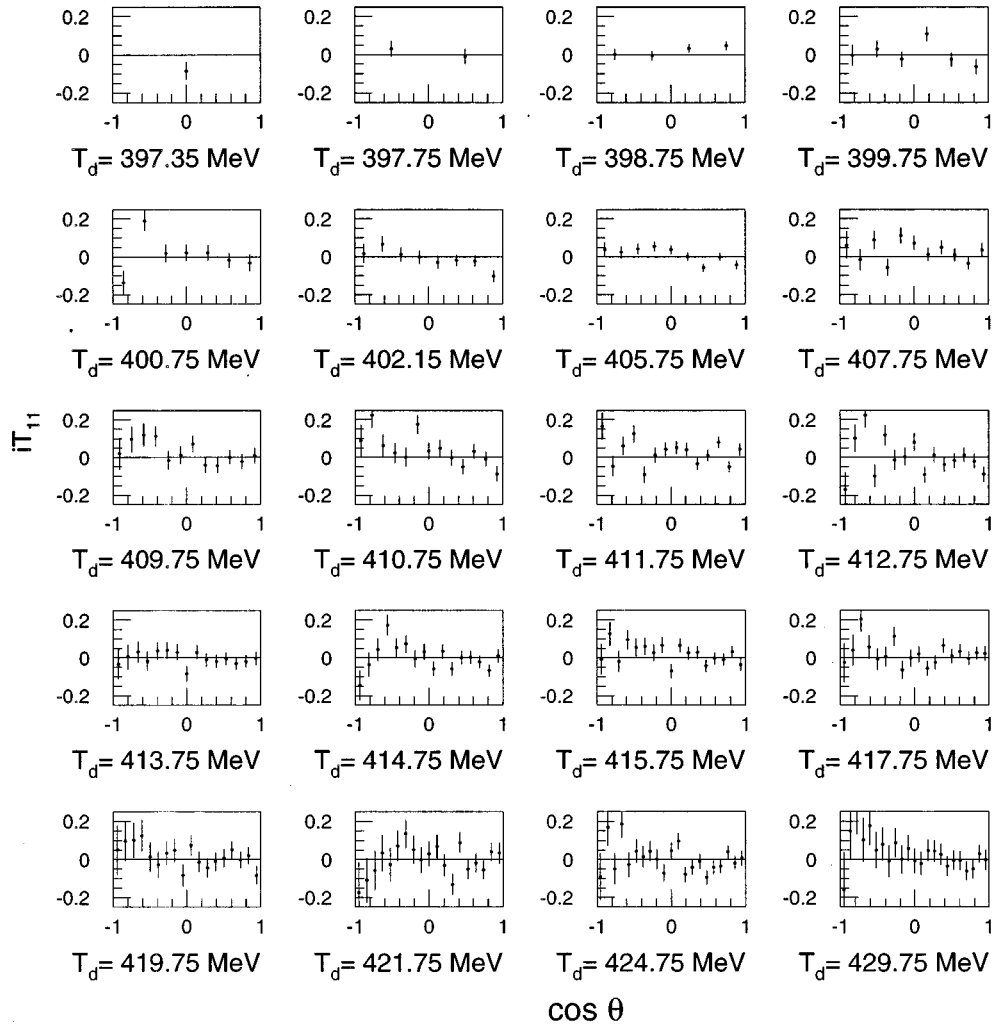
Eq. (3) in the forward and backward directions at low energies. It was assumed that a $pn \rightarrow \pi^0 d$ reaction took place on the neutron inside the initial deuteron and that the ${}^3\text{He}$ is formed in a final state interaction between the produced deuteron and the spectator proton. Such a model immediately explains the striking experimental result that $|B|^2 \ll |A|^2$ near threshold [3]. By feeding in phenomenological $pp \rightarrow d\pi^+$ amplitudes, and after including corrections from nuclear D states and small contributions from intermediate spin-singlet (d^*) states, the structure of all the IUCF [2] and LNS [3] data could be understood up to an overall constant.

The model predicts that the amplitudes A and B should be complex linear functions of η at low energies of the form

$$\begin{aligned} A &= A_0 + A_1 \eta \cos \Theta, \\ B &= B_0 + B_1 \eta \cos \Theta, \end{aligned} \quad (7)$$

though they only considered the cases where $\cos \Theta = \pm 1$.

In contrast, the present data were taken over the whole angular range. If one retains only these A and B amplitudes,

FIG. 4. Complete set of deuteron vector analyzing powers $iT_{11}(\Theta)$.

iT_{11} and T_{22} will remain identically zero at all angles, in accordance with our observations. Furthermore, to the extent that (A_0, B_0) reflect pion S -wave production and (A_1, B_1) P -wave production, then the $\cos\Theta$ in Eq. (7) should always be associated with an η factor. If this were the case, then both the amplitude squared $(p_p/p_\pi)d\sigma/d\Omega$ and the tensor analyzing power T_{20} should lie on universal curves in the global variable $\eta\cos\Theta$. Inspection of the combined data sets in Fig. 7 shows this to be a very good approximation and it is this which leads to the essential energy independence of the parameters a and b used in the spectrum fitting process of Eq. (6).

Since the data are not sensitive to the overall phases of the amplitudes, A_0 and B_0 can be taken to be real and the other terms written as $A_1 = |A_1|e^{i\phi}$ and $B_1 = |B_1|e^{i\psi}$. This led therefore to fitting the data at all energies and angles in terms of the six free parameters of Eq. (7). The B amplitude is comparatively small and slowly varying and the quality of the fit is not diminished by taking it to be constant, i.e., putting $B_1 = 0$.

The unpolarized differential cross section and tensor analyzing powers then follow from Eq. (3),

$$\frac{d\sigma}{d\Omega} = \frac{\eta m_\pi}{3p_p} (A_0^2 + 2B_0^2 + 2\eta A_0|A_1|\cos\phi\cos\Theta + |A_1|^2\eta^2\cos^2\Theta) \quad (8)$$

and

$$T_{20} \frac{d\sigma}{d\Omega} = -\frac{\sqrt{2}\eta m_\pi}{3p_p} (A_0^2 - B_0^2 + 2\eta A_0|A_1|\cos\phi\cos\Theta + |A_1|^2\eta^2\cos^2\Theta). \quad (9)$$

The best fit to all the present data, yielding a χ^2/degree of freedom of 2.0, is with parameters

$$\begin{aligned} A_0 &= (3.203 \pm 0.004) \sqrt{\mu\text{b/sr}}, \\ |A_1| &= (7.58 \pm 0.04) \sqrt{\mu\text{b/sr}}, \\ \phi &= (0.34 \pm 0.01) \text{ rad}, \\ B_0 &= (0.651 \pm 0.005) \sqrt{\mu\text{b/sr}}. \end{aligned} \quad (10)$$

Not included in the error bars are the systematic effects of 8% in absolute normalization and 3% in calibration of the

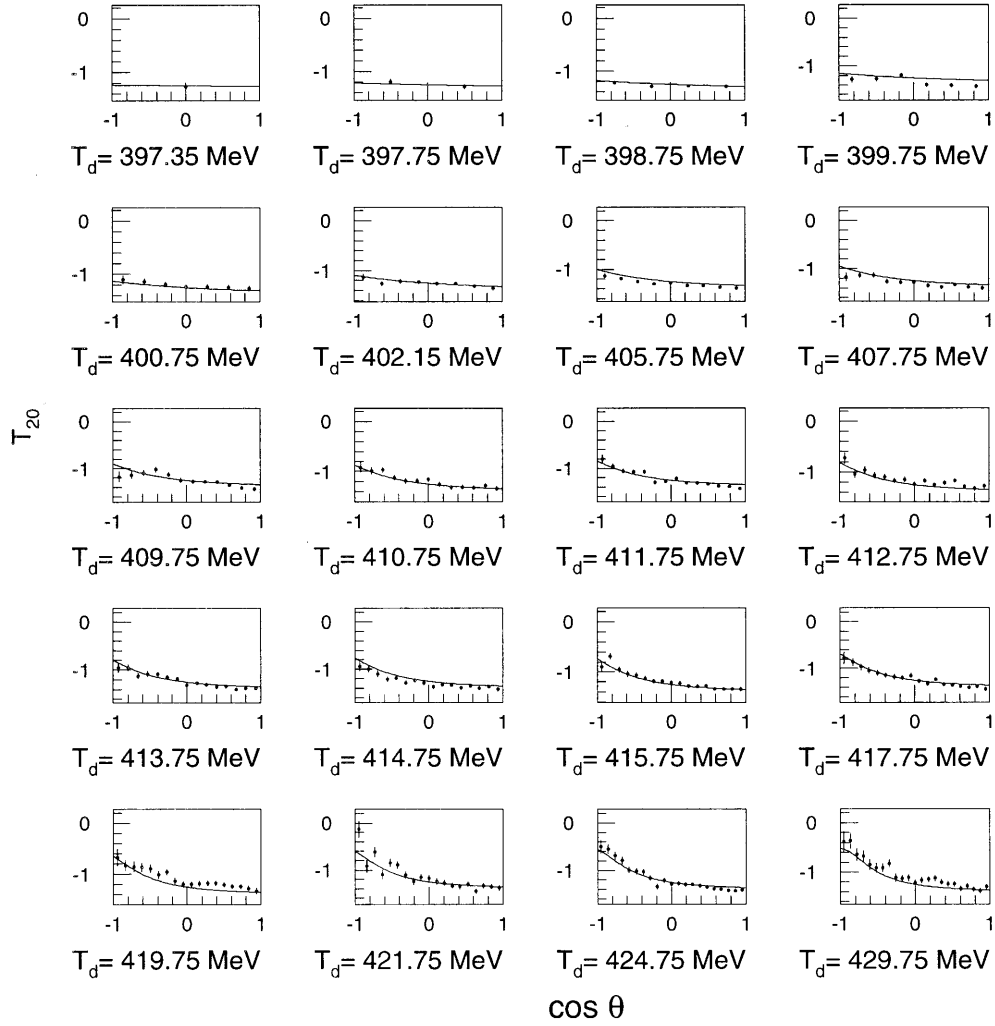


FIG. 5. Complete set of the deuteron tensor analyzing powers $T_{20}(\Theta)$ compared with curves representing the global fit of Eqs. (8) and (9).

beam polarization. It is curves corresponding to this global fit which are shown in all the figures. The description of 900 data points in terms of four real parameters is impressive.

The global fit yields a total cross section of

$$\sigma_T = \frac{4\pi}{3} \frac{m_\pi}{p_p} \eta \left(A_0^2 + 2B_0^2 + \frac{1}{3} |A_1|^2 \eta^2 \right), \quad (11)$$

so that

$$\frac{\sigma_T}{\eta} = (15.3 + 22.4\eta^2) \quad \mu\text{b}, \quad (12)$$

where the statistical error bars are negligible and account has been taken of the variation of p_p with η .

The present threshold value of $a_S \equiv \lim_{\eta \rightarrow 0} \sigma_T / \eta = (15.3 \pm 1.2) \mu\text{b}$ is in accordance with the values obtained using pionic atoms, $12.3 \pm 3.4 \mu\text{b}$ [9] and $15.8 \pm 3.6 \mu\text{b}$ [10], though these have rather large error bars.

Curiously, the value is also in agreement with the IUCF result of $15.0 \pm 1.5 \mu\text{b}$ [2], but this is due to their η^2 term in Eq. (11) being large and negative. In contrast to their find-

ings, there is no evidence up to $\eta=0.4$ of the S -wave strength decreasing with increasing energy.

The cross-section-weighted mean of the deuteron tensor analyzing power follows immediately from Eqs. (8) and (9) with the values given in Eq. (10),

$$T_{20} = -\sqrt{2} \left(1 - \frac{0.115}{1 + 1.73\eta^2} \right). \quad (13)$$

This value is very stable, varying from -1.252 at threshold to -1.286 at our largest η value, in accordance with the results presented in Table I.

Although the integrated values of cross section and analyzing powers vary smoothly with η , this is far from the case for the differential values shown in the global fits of Fig. 7. It should be noted that in the global parametrization, T_{20} is taken to be the ratio of two quadratic functions as fixed by Eqs. (8) and (9).

Germond and Wilkin only calculated in the forward and backward directions [5], but it is possible to deduce the values of the global parameters from their work:

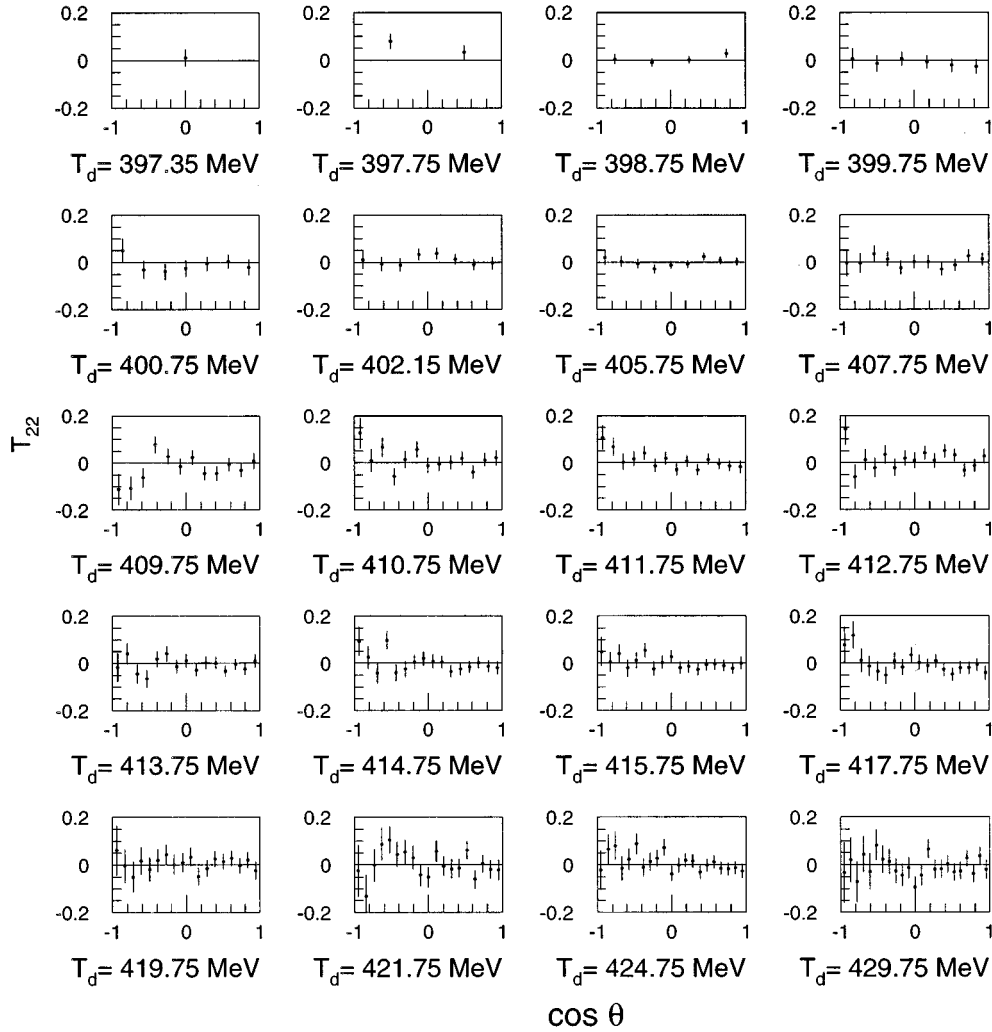


FIG. 6. Complete set of the deuteron tensor analyzing powers $T_{22}(\Theta)$.

$$\begin{aligned}
 A_0 &= 2.30 \sqrt{\mu\text{b/sr}}, \\
 |A_1| &= 5.48 \sqrt{\mu\text{b/sr}}, \\
 \phi &= 0.36 \text{ rad}, \\
 B_0 &= 0.61 \sqrt{\mu\text{b/sr}}. \quad (14)
 \end{aligned}$$

The relative sizes of A_0 and $|A_1|$ and the phase of A_1 are in complete agreement with the values quoted in Eq. (10), though the overall magnitudes are too small by a factor of 1.36. It is of course difficult to estimate with precision the absolute magnitude of the overlap form factor required in their model at momentum transfers as large as 2 fm^{-1} . Since most of the energy variation in the model comes from the underlying pion-nucleon dynamics rather than nuclear form factors, uncertainties in the form factor are less important for the ratio A_1/A_0 . On the other hand, the prediction for the small amplitude B_0 depends sensitively upon nuclear D states and the details of the $pp \rightarrow d^* \pi$ amplitudes.

VI. CONCLUSIONS

By measuring the differential cross section and three deuteron analyzing powers of the reaction $\bar{d}p \rightarrow {}^3\text{He} \pi^0$ at 20

energies with an average of 11 angles per energy, the most complete low-energy pion production experiment of its kind has been carried out.

The results are in stark contrast to the analogous near-threshold measurements of $p d \rightarrow {}^3\text{He} \eta$ [8] where no variation of the cross section with Θ was observed. Furthermore, the S -wave amplitude for η production decreases rapidly with η , as compared to essential constancy seen here for the S -wave production of pions. This contrasting behavior must be due to η production being driven by the S -wave $N^*(1535)$ while π production is dominated by P -wave Δ formation plus a nonresonant S -wave background. This combination of S - and P -wave amplitudes suggests that the data might be simple in terms of the variable $\eta \cos \Theta$ and indeed all our phase-space-modified differential cross sections and deuteron tensor analyzing power T_{20} seem to fall on universal curves when considered in terms of this variable. Both of the other analyzing powers are consistent with zero.

In the model of Germond and Wilkin [5], both of the allowed amplitudes in the forward and backward directions are linear functions of $\eta \cos \Theta$ and the agreement with their predictions is very good apart from an overall normalization discrepancy. In their model the relative phase between S -

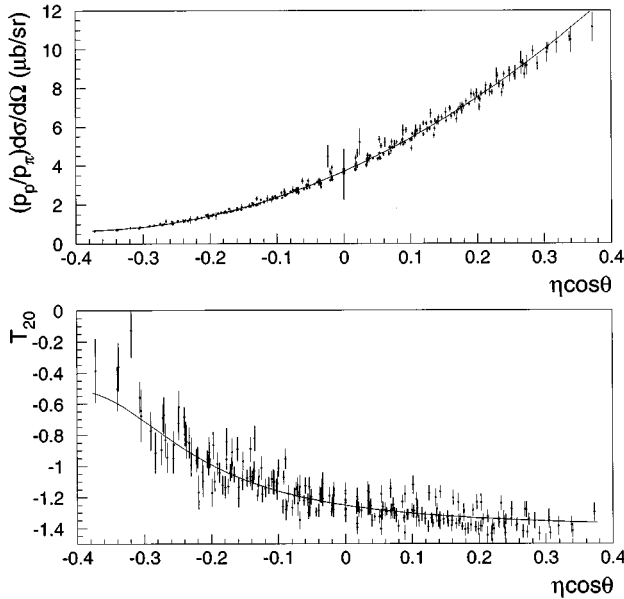


FIG. 7. Cross sections and deuteron tensor analyzing power T_{20} at all energies and angles plotted against the universal parameter $\eta\cos\Theta$ and compared with the global fit of Eqs. (8) and (9).

and P -wave pion production, which is crucial to the understanding of the angular asymmetry of the cross section and analyzing power, originates mainly from the phenomenological $pp \rightarrow d\pi^+$ amplitudes used as input to the calculation. It

is only because there is no S - and P -wave interference that the unpolarized $pp \rightarrow d\pi^+$ differential cross section is relatively smooth. The relative size of the η^2 coefficient for pion production in pd collisions determined from Eq. (11) is only 1.46 as compared to the 4.2 ± 0.4 for pp production shown in Eq. (1). Thus the fraction of P -wave cross section actually goes down as the nucleus increases in size.

To investigate the reaction further and find the relative phase of the A and B amplitudes would involve proton-deuteron spin-correlation experiments [11]. According to the interpretation presented here, such a measurement of $C_{L,L,0,0}$ is also likely to produce a global function of $\eta\cos\Theta$ at low energies.

The only other reaction where strong S - and P -wave interference is likely to be interesting at low energies is $p^3\bar{\text{He}} \rightarrow ^4\text{He}\pi^0$. Since only two complex amplitudes are involved, a measurement of the cross section, proton analyzing power, and spin-correlation parameter would be sufficient to produce a full amplitude analysis which would be a further constraint on the theoretical models of pion production.

ACKNOWLEDGMENTS

The SATURNE staff is gratefully acknowledged for the high quality beam. One of the authors (V.N.) wishes to thank his Saclay colleagues for their hospitality and is grateful to J. Arvieux, J.P. Carlos, J. Mougey, and A.A. Vorobyov for their interest and support of this work. For this research W.T.H.v.O was supported in part by the North Atlantic Treaty Organization.

-
- [1] D.A. Hutcheon, E. Korkmaz, G.A. Moss, R. Abegg, N.E. Davison, G.W.R. Edwards, L.G. Greeniaus, D. Mack, C.A. Miller, W.C. Olsen, I.J. van Heerden, and Ye Yanlin, *Phys. Rev. Lett.* **64**, 176 (1990).
- [2] M.A. Pickar, A.D. Bacher, H.O. Meyer, R.E. Pollock, and G.T. Emery, *Phys. Rev. C* **46**, 397 (1992).
- [3] A. Boudard, C. Kerboul, L. Antonuk, J. Arvieux, J. Berger, R. Bertini, M. Boivin, J.M. Durand, G. Roy, J. Tinsley, J. Yonnet, B. Mayer, and Nguyen van Sen, *Phys. Lett. B* **214**, 6 (1988); C. Kerboul, Thèse de doctorat de l'Université de Strasbourg, 1987; C. Kerboul, A. Boudard, L. Antonuk, J. Arvieux, J. Berger, R. Bertini, M. Boivin, J.M. Durand, A. Stetz, J. Tinsley, J. Yonnet, Nguyen van Sen, Ye Yanlin, B. Mayer, J. Cameron, C. Lapointe, D.M. Sheppard, J.F. Germond, and C. Wilkin, *Phys. Lett. B* **181**, 28 (1986).
- [4] F. Plouin, in *Production and Decay of Light Mesons*, edited by P. Fleury (World Scientific, Singapore, 1988), p. 114.
- [5] J.-F. Germond and C. Wilkin, *J. Phys. G* **16**, 381 (1990).
- [6] J. Arvieux, S.D. Backer, A. Boudard, J. Cameron, T. Hagesawa, D. Hutcheon, C. Kerboul, G. Gaillard, and Nguyen Van Sen, *Nucl. Instrum. Methods A* **273**, 48 (1988).
- [7] H. Quéchon, Thèse de doctorat de l'Université d'Orsay, 1980.
- [8] B. Mayer, A. Boudard, B. Fabbro, M. Garçon, C. Kerboul, J. Poitou, F. Wellers, J. Saudinos, E. Tomasi-Gustafsson, J.P. Mouly, R.S. Kessler, B.M.K. Nefkens, B. Tippens, A. van der Schaaf, R. Abegg, W.T.H. van Oers, W. Briscoe, A. Petrov, W.W. Jacobs, and A. Moalem, *Phys. Rev. C* **53**, 2068 (1996).
- [9] I. Schwanner, R. Abela, G. Backenstoss, W. Kowald, P. Pavlopoulos, L. Tauscher, H.-J. Weyer, P. Blüm, M. Dörr, W. Fletscher, D. Gotta, R. Guigas, H. Koch, H. Poth, G. Schmidt, and H. Ulrich, *Phys. Lett.* **96B**, 268 (1980); I. Schwanner, G. Backenstoss, W. Kowald, L. Tauscher, H.-J. Weyer, D. Gotta, and H. Ulrich, *Nucl. Phys.* **A412**, 253 (1984).
- [10] G.R. Mason, G.A. Beer, M.S. Dixit, S.K. Kim, J.A. Macdonald, A. Olin, R.M. Pearce, W.C. Sperry, and J.S. Vincent, *Nucl. Phys.* **A340**, 240 (1980).
- [11] V.P. Ladygin and N.B. Ladygina, *Yad. Fiz.* **58**, 1365 (1995) [*Phys. At. Nucl.* **58**, 1283 (1995)].